Available online at www.sciencedirect.com
SCIENCE DIRECT®
Polymer 44 (2003) 7721–7727
polymer
www.elsevier.com/locate/polymer

Synthesis and characterization of polystyrene-*block*-polyisoprene nanofibers with different crosslinking densities

Guojun Liu*, Zhao Li, Xiaohu Yan

Department of Chemistry, University of Calgary, 2500 University Drive, NW, Calgary, Alta, Canada T2N 1N4

Received 9 July 2003; received in revised form 25 September 2003; accepted 6 October 2003

Abstract

Polystyrene-*block*-polyisoprene or PS-*b*-PI with 74 styrene and 230 isoprene units was prepared by anionic polymerization. The diblock formed cylindrical micelles with PI core and PS corona in a PS-selective solvent *N*,*N*-dimethylacetamide. Nanofibers with different crosslinking densities were obtained after PI core crosslinking with differing amounts of sulfur monochloride. The nanofibers were characterized by elemental analysis, FTIR, transmission electron microscopy, and light scattering.

Keywords: Block copolymers; Nanofibers; Cylindrical micelles

1. Introduction

By the fine-tuning of the relative length of a diblock copolymer, one can prepare cylindrical micelles from the copolymer in a block-selective solvent [1–4]. The core of the cylindrical micelles can be crosslinked to yield crosslinked cylindrical micelles or nanofibers [5,6]. In bulk, block copolymers self-assemble forming various intricate nanometer-sized block segregation patterns [7]. At the volume fraction of ~30%, the minority block of a diblock normally forms hexagonally-packed cylinders dispersed in the continuous matrix of the majority block [4]. Nanofibers are obtained by crosslinking the minority block and separating the hairy cylinders via solvent dispersion [8–11].

Diblock copolymer nanofibers (BCN) possess a crosslinked cylindrical core of one block and a corona of another block (Scheme 1). Dilute BCN dispersions or 'solutions' are thermodynamically stable and each BCN is a giant molecule. BCNs may be viewed as supra-polymer chains [12]. In the previous papers in this series [13,14], we described the preparation of nanofibers from block-segregated films of polystyrene-*block*-polyisoprene or PS-*b*-PI, where PI formed the minority or crosslinking block. We also reported the separation of the nanofibers into fractions with average lengths from several hundred nanometers to several micrometers and the characterization of the fractions by light scattering and viscometry. The zero-shear intrinsic viscosity data of the nanofiber fractions agreed with the Yamaka-Fujii-Yoshizaki theory [15,16] developed originally for wormlike polymer chains.

The PS-*b*-PI nanofibers we used before were highly crosslinked and it was difficult to prepare uniformly crosslinked nanofibers with a low crosslinking degree from the solid-state synthesis approach. The use of the crosslinking agent sulfur monochloride, S_2Cl_2, as the limiting agent would have lead to preferential crosslinking of the PI domains in the film surfaces and yielded nanofibers with a range of crosslinking densities. In this paper, we report on the preparation of nanofibers with PI double bond conversions P_{PI} of 25, 45, and 71% by reaction of various amounts of S_2Cl_2 with PS-*b*-PI cylindrical micelles formed in *N*,*N*-dimethylacetamide, DMAC.

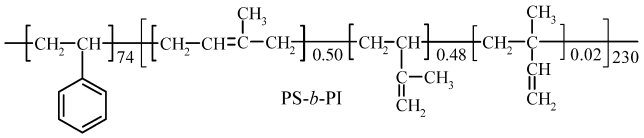

We also report on the results of nanofiber characterization by a range of techniques including transmission electron microscopy (TEM) and light scattering.

* Corresponding author. Tel.: +1-403-2205343; fax: +1-403-2899488.
E-mail address: gliu@ucalgary.ca (G. Liu).

0032-3861/$ - see front matter © 2003 Elsevier Ltd. All rights reserved.
doi:10.1016/j.polymer.2003.10.004

Scheme 1. Schematic illustration of the structure of a diblock nanofiber in solvent.

2. Experimental section

2.1. Materials

Unless stated otherwise all chemicals were purchased from Aldrich. Isoprene was distilled in the presence of *n*-butyl lithium and styrene was purified by double distillation first over CaH_2 and then in the presence of benzylmagnesium chloride. Tetrahydrofuran (THF) was refluxed over potassium/benzophenone for at least 1 day and distilled before use. Cyclohexane was refluxed over potassium and distilled before use. DMAC was dried by stirring overnight at 130 °C with BaO and then distilled under reduced pressure. Sulfur monochloride was used as received.

2.2. Polymer synthesis and characterization

Polymer PS-*b*-PI was prepared by living anionic polymerization in cyclohexane with ~1 vol.% of THF at 45 °C [17]. Styrene and isoprene were polymerized for 4 and 17 h, individually. Polymerization was terminated by addition of degassed methanol. The diblock prepared was purified by precipitation into ethanol and dried at room temperature under vacuum.

The diblock was characterized by ^{1}H NMR, size exclusion chromatography (SEC), and light scattering (LS). SEC analysis was performed using a Styragel HT-4 broadband column (Waters) calibrated with poly(methyl methacrylate) standards. The eluant used was THF. Light scattering was done using a Brookhaven model 9025 instrument equipped with a 632.8 nm He–Ne laser. The difference, Δn_r, between the refractive index of a diblock THF solution and THF was determined using a differential refractometer (Precision Instruments Co.) with light that had passed a bandpass filter centered around 633 nm. The specific refractive index increments, dn_r/dc, were determined from the intercept of a $\Delta n_r/c$-vs.-c plot, where c denotes polymer concentration [18].

2.3. Nanofiber preparation and purification

After some stirring, the PS-*b*-PI diblock dispersed directly in dry DMAC at 3 mg/ml. According to Price [1], this diblock should form mainly cylindrical micelles with PI cores and PS shells. Sulfur monochloride at 0.30, 0.45, and 0.60 molar ratios to isoprene, were then added and stirred with the cylindrical micelles to yield three-nanofiber samples X1, X2, and X3. To separate the nanofibers from co-existing nanospheres, methanol, ~30 vol.%, was added slowly under vigorous stirring into the crosslinked sample until the solution just turned turbid. The mixture was then left to stand overnight to precipitate the nanofibers. The purification was repeated if deemed necessary after sample purity examination by TEM. The purified nanofibers were redispersed and stored in THF.

2.4. Transmission electron microscopy

TEM was used to obtain the length distribution of the nanofibers and to estimate the diameter of the PI cores. To obtain the TEM images of the nanofibers, the fiber dispersions in THF were aspirated on to carbon-coated copper grids using a home-built device [19]. The fibers were then stained with OsO_4 vapor for 4 h before viewing by a Hitachi-7000 electron microscope operated at 75 kV.

2.5. Light scattering study

Nanofibers at $\sim 5 \times 10^{-6}$ g/ml in THF was dispensed in a vial with a special lid. The lid contained a gas inlet fitted with a 0.1 μm filter and an outlet fitted with a polyethylene tube. After centrifugation at 2500*g* for 30 min, the vial was carefully taken out and secured in a clamp. Pressure was applied through a syringe connected to the filter to push out the nanofiber solution via the polyethylene tube that hang half-way into the nanofiber solution. After discarding the initial portion, the middle fraction was dispensed into a clean cylindrical quartz cell with a diameter of 2.5 cm for light scattering measurements. A total of 19 angles starting at 12° were used in each measurement. For low angle data, the angle increment used was 1°. For scattering in the full angle range, the angles used were 12, 14, 16, 18, 20, 22, 24, 30, 40, 50, 60, 70, 80, 90, 100, 110, 120, 130, and 140°, respectively. To ensure data precision, light intensities at each concentration were measured once in a low to high angle scan and another time in a high to low angle scan and the intensities in the two scans at each angle were averaged. The instrument used was of Brookhaven model BI-200SM.

3. Results and discussion

3.1. Polymer characterization

Fig. 1 shows a ^{1}H NMR spectrum of PS-*b*-PI in $CDCl_3$. From the intensity ratio of the vinyl proton peaks at 5.7, 4.7, and 5.1 ppm we estimated the relative contents of 2, 48, and 50% for 1,2-, 3,4-, and 1,4-addition products for PI [20]. The intensity ratio of the vinyl proton peaks between 4.7 and 5.7 ppm to those of PS between 6.6 and 7.3 ppm yielded $n/m = 0.32$. The weight-average molar mass M_W determined using the specific refractive index dn_r/dc of 0.147 ml/g was 2.36×10^4 g/mol for the diblock. Combining the

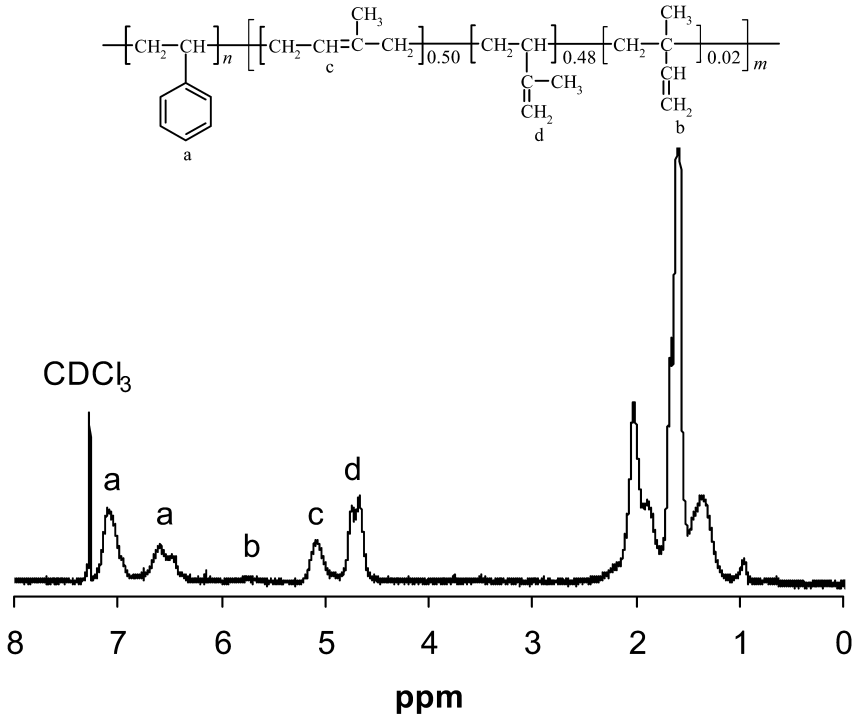

Fig. 1. Proton NMR spectrum of PS-*b*-PI.

NMR and light scattering data, we calculated the weight-average repeat units of 74 for styrene and 230 for isoprene (Table 1). The polydispersity index was low at 1.05.

Fig. 2(a) shows a FTIR spectrum of the diblock. A weak peak at 1665 cm^{-1}, characteristic of 1,4-*cis* microstructure, and a strong peak at 840 cm^{-1}, characteristic of 1,4-*trans* microstructure, suggest that the 1,4-addition product was mostly in the *trans* form [21]. The peaks at 890 and 1645 cm^{-1} are characteristic of the 3,4-addition product.

3.2. Crosslinking reaction

Nanofiber preparation involved cylindrical micelle formation from the diblock in DMAC and then the crosslinking of the PI cores with S_2Cl_2 [22]. The occurrence of the above reaction can be judged from intensity decrease for peaks at 840, 890, and 1642 cm^{-1}, respectively, in Fig. 2. A quantitative analysis using the 697 cm^{-1} peak for the mono-substituted phenyl ring as reference yielded double bond conversions P_{PI} of 25, 45, and 71% for X1, X2, and X3, respectively. We have also performed elemental analysis of the samples. The number of moles of S_2Cl_2 reacted with each mole of isoprene, $[S_2Cl_2]/[I]$, was calculated for each sample from both carbon and hydrogen contents with results given in Table 2. The fact that the average $[S_2Cl_2]/[I]$ value determined from carbon and hydrogen content analyses is approximately half of P_{PI} determined from FTIR for each sample suggests that most of the S_2Cl_2 molecules participated in the bridging reaction of Scheme 2. The bridging reaction can take place between isoprene units of different chains or those of the same chain. In the core, we expect efficient inter-chain mixing and the crosslinking density should roughly equal to $(1/2)P_{PI}$.

3.3. TEM results

Fig. 3(a) shows a TEM image of a nanofiber X3 sample aspirated from THF and stained with OsO_4. Similar TEM images were obtained for the X2 nanofibers. The samples consist mostly of crosslinked cylindrical micelles co-existing with some crosslinked spherical micelles. For physical studies, the nanofibers were fractionated following procedures described in Section 2. Fig. 3(b) shows a TEM image of a fractionated X3 sample. The relative population of the crosslinked spherical micelles has decreased considerably, suggesting the effectiveness of the fractionation procedure.

Fig. 3(c) shows a TEM image of nanofiber X1. Coiled and wormlike configurations, with the latter exemplified by

Table 1
Characteristics of PS-*b*-PI

Polymer	dn_r/dc (ml/g)	M_W (g/mol) LS	M_w/M_n SEC	*n*/*m* NMR	1,4-content NMR	*n*	*M*
PS-*b*-PI	0.147	23600	1.05	0.32	50%	74	230

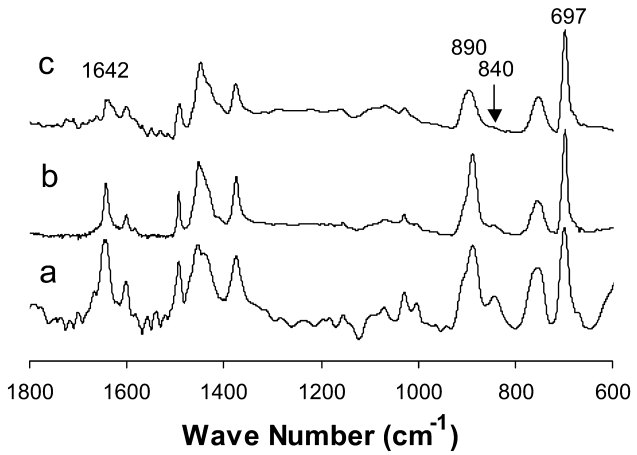

Fig. 2. FTIR spectra of PS-*b*-PI nanofibers at the PI double bond conversion of 0% (a), 25% (b), and 71% (c).

the straight nanofiber section stretching out from the bottom coil, coexist for this sample.

The lengths of more than 500 fibers for both X2 and X3 were measured manually from the TEM images and the results are summarized in Fig. 4. The term $N(L_i)$ in the figure is the number of fibers with length between $(1/2)\times(L_i + L_{i-1})$ and $(1/2)(L_i + L_{i+1})$. Using the length distribution data, we computed the number-average length, L_N, and weight-average length, L_W, of X2 and X3 with results given in Table 3. The L_W and L_N values were independent of P_{PI}. This is reasonable, because nanofiber structure should not mutate above a critical P_{PI} above which the micellar structure got locked in.

We could not obtain the length distribution function for X1 as this sample coiled and entangled much. We, however, expect its length distribution function to be similar as those of X2 or X3.

We also estimated the diameter of the nanofibers from TEM images at much higher magnifications. Since the samples were stained with OsO_4, only the PI core was seen. In each case, the PI core diameter, d_{PI}, of at least 20 nanofibers was measured. The average values are 36.9 ± 1.4, 26.6 ± 1.7, and 23.5 ± 2.2 nm for X1, X2, and X3, respectively. A decrease in d_{PI} with increasing P_{PI} suggests that the swollen state of the core in THF was at least partially retained after sample aspiration and drying.

The variation of d_{PI} and invariance of L_N with P_{PI} presents a paradox. This paradox is readily resolved by realizing a possible non-uniform swelling of nanofibers along the radial and axial directions. A fiber swells probably more readily along the radial direction, because most of the chains are oriented along this direction.

Table 2
Chemical characteristics of the nanofiber samples

Sample	Elemental analysis results				FTIR double bond conversion (%)
	C%	$[S_2Cl_2]/[I]$ from C%	H%	$[S_2Cl_2]/[I]$ from H%	
X1	75.70	0.137	9.01	0.118	25
X2	70.21	0.207	8.59	0.160	45
X3	60.11	0.368	7.30	0.321	71

A much larger d_{PI} for the dry X1 fibers explains why this sample coiled more than the X2 and X3 fibers in the dry state. After the aspiration of a nanofiber solution, many small droplets containing nanofibers land on a carbon film. Solvent evaporation starts from the outer periphery of a solvent droplet. A nanofiber may travel with the solvent front and fold or coil concurrently. The exact conformation that a nanofiber takes depends on, among other factors, the balance between the surface energy derived from the formation of a continuous PS film on the PI core surface and the bending energy of the PI core. The X1 fibers have a considerably larger PI diameter and the PS chains are thus farther apart. This does not facilitate PS chain interpenetration and film formation. The drive for PS film formation causes the PI core to coil and it coils because of the lower PI crosslinking density and thus a lower bending modulus. The other fibers do not coil as much because of their higher bending modulus.

3.4. Light scattering data treatment

Light scattering data should be treated in general by:

$$Kc/\Delta R_\theta = \frac{1}{M_W P_z(\theta)} + 2A_2 c \qquad (1)$$

where c denotes nanofiber concentration; ΔR_θ is the Rayleigh ratio; A_2 is the second Virial coefficient; K is the optical constant of the system; and $P_z(\theta)$ is the z-average scattering factor for the nanofibers. Using Eq. (1) and extrapolating to zero concentration yields $1/(M_W P_z(\theta))$ from light scattering data.

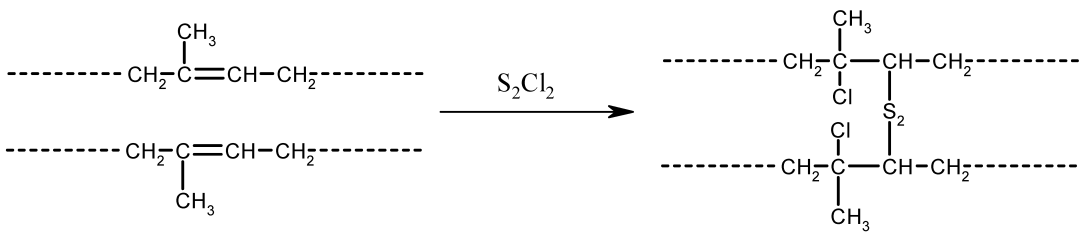

Scheme 2.

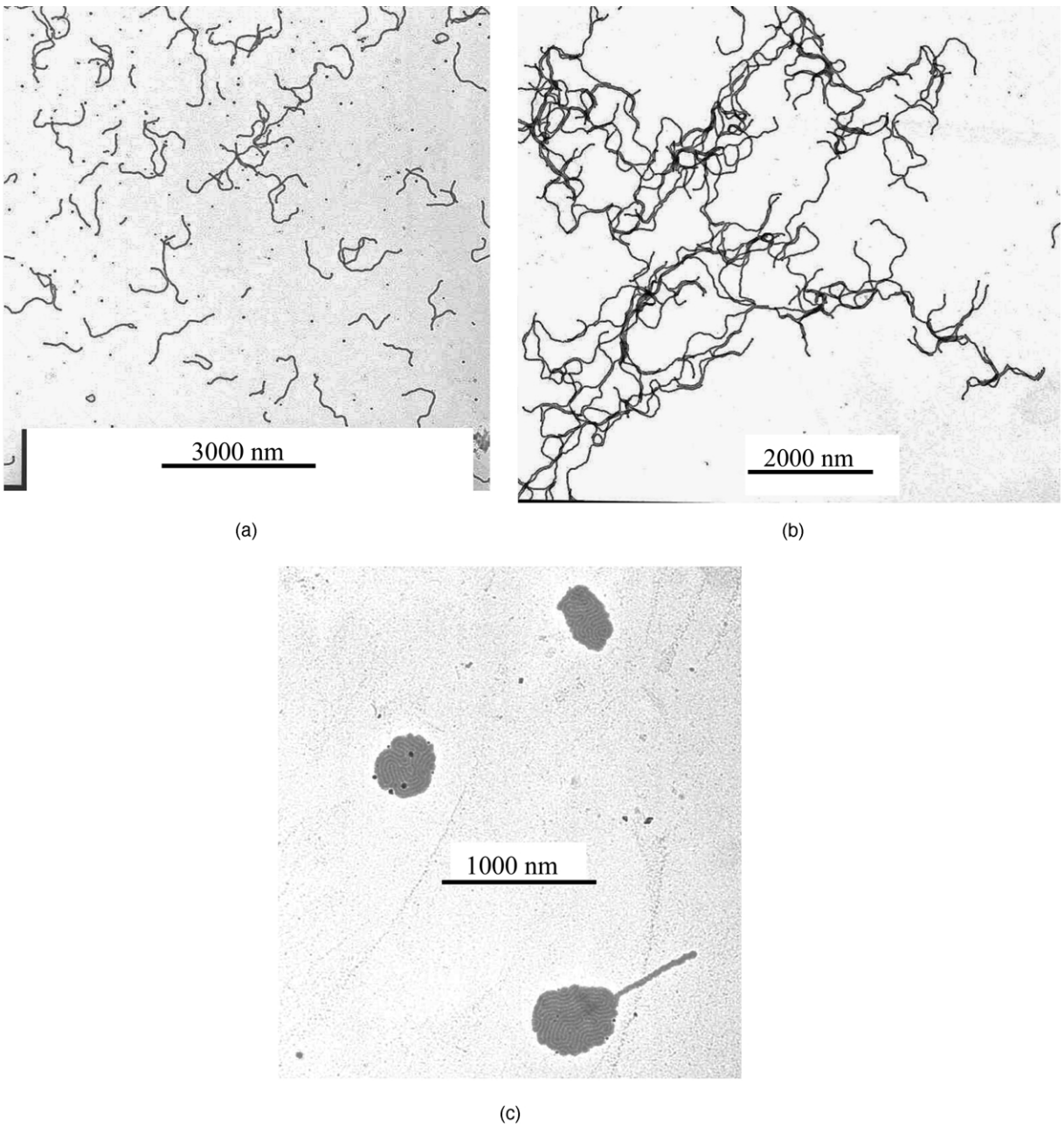

Fig. 3. TEM images of purified X3 nanofibers before (a) and after (b) nanosphere separation. Also shown is a TEM image of (c) X1 nanofibers.

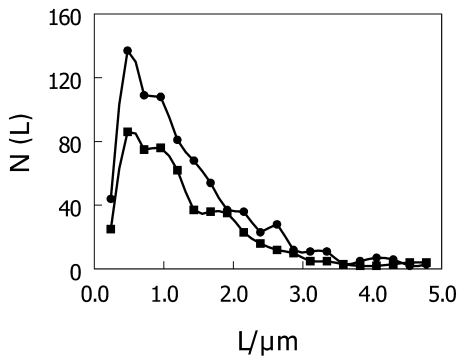

Fig. 4. Fiber population plotted as a function of length for sample X2 (■) and X3 (●), respectively.

At low scattering angles θ for which

$$qR_G/\sqrt{3} < 1 \quad (2)$$

where R_G denotes the z-average radius of gyration of the nanofibers, $P_z(\theta)$ of Eq. (1) can be expanded as a truncated series to yield the model-independent form:

$$\frac{Kc}{\Delta R_\theta} = \frac{1}{M_W}[1 + (1/3)q^2R_G^2 - B_3q^4R_G^4 + \cdots] + 2A_2c \quad (3)$$

where B_3 is a fitting constant and the magnitude of the

Table 3
Physical characteristics of the PS-*b*-PI nanofiber fractions

Sample	TEM L_W (nm)	TEM L_N (nm)	TEM d_{PI} (nm)	dn_r/dc (ml/g)	M_w (g/mol)	R_G (nm)	M_U (g/(mol nm))	SLS L_W (nm)
X1			36.9 ± 1.4	0.144	$(2.79 \pm 0.02) \times 10^8$	441 ± 1	1.55×10^5	1800
X2	1930	1310	26.6 ± 1.7	0.148	$(3.53 \pm 0.06) \times 10^8$	443 ± 1	2.00×10^5	1770
X3	1920	1280	23.5 ± 2.2	0.169	$(4.88 \pm 0.02) \times 10^8$	467 ± 7	2.65×10^5	1840

scattering wave vector q is given by

$$q = \frac{4\pi n_0}{\lambda} \sin(\theta/2) \tag{4}$$

Using Eq. (3) and extrapolating to zero concentration and zero angle yields $1/M_W$. The R_G value is obtained from θ dependence of the light scattering data at $c \to 0$.

3.5. Scattering data in the full angle range

Fig. 5(a) shows light scattering data $Kc/\Delta R_\theta$ plotted vs. $[\sin^2(\theta/2) + kc]$ for X2 in the full angle range, where the arbitrary plotting constant k is 2×10^5. Extrapolation of the $Kc/\Delta R(\theta)$ data to zero concentration yielded $1/(M_W P_z(\theta))$ denoted by the centers of the hollow circles in Fig. 5(a).

Function $P_z(\theta)$ or $P_z(q)$, governed by the relative positions or the distribution of the scattering sub-units in a particle, is called the scattering structural factor. There have been many theoretical studies of $P_z(\theta)$ for wormlike polymer chains or surfactant cylindrical micelles with a negligible [23–25] or significant [26,27] cross-section.

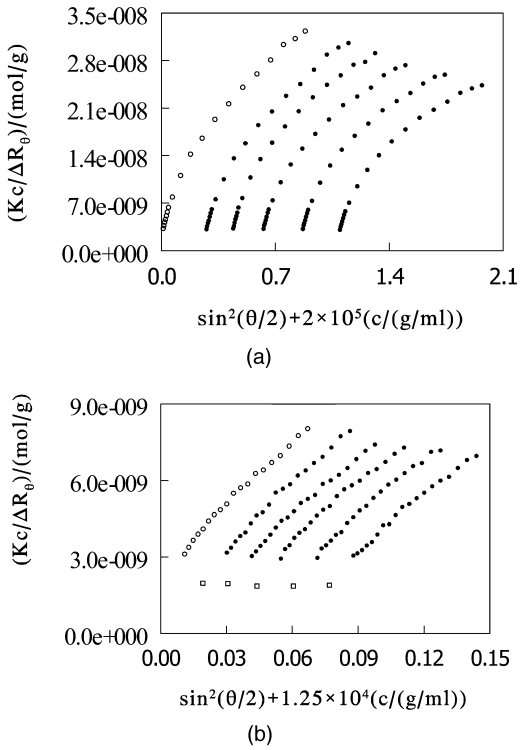

Fig. 5. Zimm plots for nanofiber sample X2 in the scattering angle range of (a) 12–140° and (b) 12–30°.

Regardless of the cross-section, the $P_z(q)$ function of long fibers is rich in characteristic features only in the low q region. This is especially true for our fibers with length larger than 1 μm. Unfortunately, our instrument does not allow us to access the low q region. For lack of key features in the low q region, we will not fit the experimental $P_z(q)$ data with complex theoretical equations. Rather, we will use the $P_z(q)$ data in the high q region only to determine the molar mass M_U of unit-length nanofibers.

Light scattering probes structural feature on the length scale of $\sim 1/q$. Above a sufficiently large q, the probing distance is shorter than the persistence length l_P and the scattering behavior of a nanofiber resembles that of a rigid rod. An infinitely thin rod shows the high-q asymptotic behavior:

$$P_z(\theta) = \frac{\pi}{qL_W} \tag{5a}$$

or

$$Kc/\Delta R_\theta|_{c\to 0} = \frac{qL_W}{\pi M_W} = \frac{q}{\pi M_U} \tag{5b}$$

Thus, the $Kc/\Delta R_\theta|_{c\to 0}$ values at the high q end enable M_U evaluation.

The finite cross-section of a fiber modifies $P_z(q)$ in the high q region. According to Jerk et al. [28]

$$P_z(q) = \left(\frac{\pi}{qL_W}\right) P_{CS}(q) \tag{6}$$

where $P_{CS}(q)$, the cross-section scattering function, can be calculated from an expression approximated by us [9] by assuming a uniform cross-section for fibers. A rough calculation indicated that $P_{CS}(q)$ was close to 1 for all q values used. Therefore, we neglected $P_{CS}(q)$ in our subsequent discussion.

According to Denkinger and Burchard [29], the best way to present the $P_z(q)$ data is to use the bending plot or to plot $qP_z(q)$ as a function of q. A variation of such a plot is shown in Fig. 6, which plots $qP_z(q)M_W$ or $q\Delta R_\theta/Kc|_{c\to 0}$ as a function of q for samples X1, X2, and X3. The data seemed to peak around 0.005 nm^{-1} and then level off to the rigid-rod asymptotic behavior in qualitative agreement with the wormlike polymer chain behavior [29]. Using the leveled $qP_z(q)M_W$ values and Eq. (5b), we obtained the M_U values of 1.55 ×, 2.00 ×, and 2.65×10^5 g/(mol nm) for X1, X2, and X3, respectively.

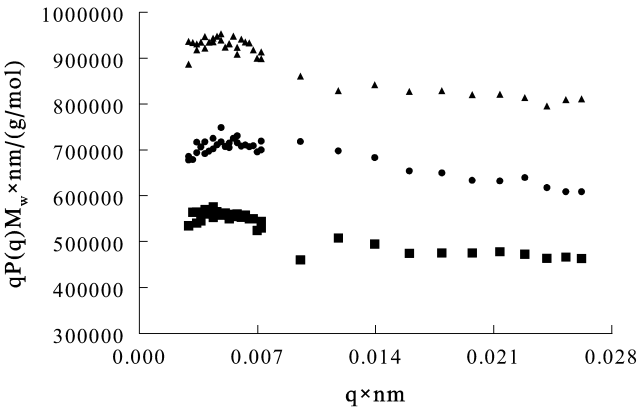

Fig. 6. Plot of $qp(q)M_W$ as a function of q for X1 (■), X2 (●), and X3 (▲), respectively. The data look more crowded at the low q end, because the low angle data were plotted as well.

3.6. Low-angle scattering data

Fig. 5(b) plots the scattering data obtained between 12 and 30° for X2 in THF. The open circles and squares represent data extrapolated to zero concentration and angle, respectively, by the instrument software using Eq. (3). Extrapolation to zero angle and zero concentration yielded $M_W = 3.5 \times 10^8$ g/mol and the θ dependence of the data denoted by the open circles yielded $R_G = 443$ nm. We have treated the data of Fig. 5(a) in the 12–30° range also and the M_W and R_G values reported in Table 3 are the averages from the two sets of scattering data. The M_W and R_G values of other samples were obtained similarly and the small deviations in M_W and R_G suggest high data precision.

The LS M_W value increases with P_{PI} for the samples because of incorporation of more S_2Cl_2 into the nanofiber core with increasing P_{PI}. Combining the M_W and M_U values, we calculated L_W. These values are listed in the last column of Table 3. The good agreement between the L_W values determined from LS and those from TEM renders validity to the scattering results. The fact that the LS L_W value of X1 is between those of X2 and X3 suggests that the X1 sample probably had a similar length distribution as the other samples.

The R_G values are typically ~450 nm for the nanofibers. We are less confident about the accuracy of the R_G values, because Eq. (2) is valid for X3 with $R_G = 467$ nm only for scattering angles less than 15°. Regardless, the trend that R_G increased somewhat with P_{PI} agrees with the expectation that nanofiber rigidity increased with P_{PI}.

4. Conclusions

A PS-*b*-PI sample has been prepared by anionic polymerization. The diblock formed cylindrical micelles in DMAC. Nanofibers with different crosslinking densities were prepared by reaction of various amounts of S_2Cl_2 with the cylindrical micelles. TEM and LS were used to characterize the nanofiber samples. The agreement between the TEM and LS L_W values suggests the validity of the LS M_w values. The R_G value variation trend and the TEM images of the dry nanofibers suggested an expected nanofiber rigidity increase with increasing PI crosslinking density.

Acknowledgements

The authors would like to thank NSERC of Canada for financial support of this research.

References

[1] Price C. Pure Appl Chem 1983;55:1563.
[2] Zhang LF, Eisenberg A. Science 1995;268:1728.
[3] Ding JF, Liu GJ, Yang ML. Polymer 1997;38:5497.
[4] Raez J, Barjovanu R, Masseay JA, Winnik MA, Manners I. Angew Chem Int Ed 2000;39:3862.
[5] (a) Tao J, Stewart S, Liu GJ, Yang ML. Macromolecules 1997;30: 2738. (b) Stewart S, Liu GJ. Angew Chem Int Ed 2000;39:340. (c) Liu FT, Liu GJ. Macromolecules 2001;34:1302.
[6] Won Y-Y, Davis HT, Bates FS. Science 1999;283:960.
[7] For block segregation patterns see, for example, Bates FS, Fredrickson GH. Phys Today 1999 February issue;32.
[8] (a) Liu GJ, Qiao L, Guo A. Macromolecules 1996;29:5508. (b) Liu GJ. Adv Mater 1997;9:437.
[9] Liu GJ, Ding J, Qiao L, Guo A, Gleeson JT, Dymov B, Hashimoto T, Saijo K. Chem Eur J 1999;5:2740.
[10] Massey J, Power KN, Manners I, Winnik MA. J Am Chem Soc 1998; 120:9533.
[11] (a) Yan XH, Liu GJ, Liu FT, Tang BZ, Peng H, Pakhomov AB, Wong CY. Angew Chem Int Ed 2001;40:3593. (b) Yan XH, Liu GJ, Liu FT. Macromolecules 2001;34:9112.
[12] Liu GJ, Yan XH, Qiu XP, Li Z. Macromolecules 2002;35:7742.
[13] Liu GJ, Yan XH, Duncan S. Macromolecules 2002;35:9788.
[14] Liu GJ, Yan XH, Duncan S. Macromolecules 2003;36:2049.
[15] Yamakawa H, Fujii M. Macromolecules 1974;7:128.
[16] Yamakawa H, Yoshizaki T. Macromolecules 1980;13:633.
[17] See, for example, Ren Y, Lodge TP, Hillmyer MA. Macromolecules 2000;33:866.
[18] Huglin MB. Light scattering from polymer solutions. London: Academic Press; 1972.
[19] Ding JF, Liu GJ. Macromolecules 1999;32:8413.
[20] Morton M. Anionic polymerization: principles and practice. New York: Academic Press; 1983.
[21] Miyaki Y, Nagamatsu H, Iwata M, Ohkoshi K, Se K, Fujimoto T. Macromolecules 1984;17:2231.
[22] Glazer J. J Polym Sci 1954;14:225.
[23] Koyama R. J Phys Soc Jpn 1973;34:1029.
[24] Yoshizaki T, Yamakawa H. Macromolecules 1980;13:1518.
[25] Porod G. J Polym Sci 1953;10:157.
[26] Pedersen JS, Schurtenberger P. Macromolecules 1996;29:7602.
[27] Sharp P, Bloomfield VA. Biopolymers 1968;6:1201.
[28] Jerke G, Pedersen JS, Egelhaaf SU, Schurtenberger P. Phys Rev E 1997;56:5772.
[29] Denkinger P, Burchard W. J Polym Sci: Part B, Polym Phys 1991;29: 589.